



## Research paper

Synthesis and coordination chemistry of sterically hindered cobalt(II)  $\beta$ -ketoiminate complexes

Suman Debnath\*, Navamoney Arulsamy, Mark P. Mehn

Department of Chemistry, University of Wyoming, 1000 E. University Avenue, Laramie, WY 82071, United States

## ARTICLE INFO

## Keywords:

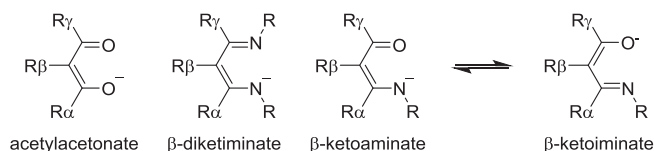
$\beta$ -Ketoiminate ligand  
Cobalt(II) complex  
X-ray crystallography  
Magnetic susceptibility

## ABSTRACT

The reactions of cobalt(II) chloride with  $\alpha,\beta$ -unsaturated- $\beta$ -ketoamines,  $\text{CH}_3\text{C}(\text{=O})\text{CH}=\text{C}(\text{NHR})\text{CH}_3$ , where  $\text{R} = \text{-phenyl, HL}^{\text{Ph}}$ ;  $\text{R} = \text{-mesityl, HL}^{\text{mes}}$ ;  $\text{R} = \text{-2,6-diisopropylphenyl, HL}^{\text{dipp}}$ , and sodium hydride in THF solvent under anaerobic conditions affords brown or orange crystals of  $\text{Co}(\text{L}^{\text{Ph}})_2$ ,  $\text{Co}(\text{L}^{\text{mes}})_2$  and  $\text{Co}(\text{L}^{\text{dipp}})_2$ , respectively. In THF/acetonitrile solvent mixture, the complexation reactions are not successful as unreactive salts containing networks of acetonitrile-coordinated sodium cations and the respective anions are formed. One of them, the sodium salt of  $\text{HL}^{\text{dipp}}$ , is isolated and characterized as  $[\text{Na}(\text{L}^{\text{dipp}})(\text{CH}_3\text{CN})]_4$ . Single-crystal X-ray diffraction data for the cobalt(II) complexes reveal that the metal centers assume distorted tetrahedral geometries. The degree of distortion increases with the size of the substituents present in the phenyl groups:  $\text{Co}(\text{L}^{\text{Ph}})_2 < \text{Co}(\text{L}^{\text{mes}})_2 < \text{Co}(\text{L}^{\text{dipp}})_2$ . Crystallographic data measured at 296, 200, 150 and 100 K for  $\text{Co}(\text{L}^{\text{dipp}})_2$  reveal that it exists as two geometrical forms, namely, distorted tetrahedral and distorted square-planar. The data also indicate that the pseudo-tetrahedral to distorted square-planar transition is favored at lower temperatures. Electrochemical data measured in THF and DCM solvents reveal the likely presence of Co(II)-solvent interaction in  $\text{Co}(\text{L}^{\text{Ph}})_2$  and  $\text{Co}(\text{L}^{\text{mes}})_2$  and no such interaction in  $\text{Co}(\text{L}^{\text{dipp}})_2$ . Magnetic susceptibility data for  $\text{Co}(\text{L}^{\text{dipp}})_2$  in the 4–300 K temperature region reveal spin-crossover at ca. 130 K. Qualitatively, the magnetic and crystallographic data complement each other with respect to the presence of the high spin pseudo-tetrahedral and low spin pseudo-square planar geometries.

## 1. Introduction

The  $\beta$ -ketoiminate bidentate ligand has many similarities to both the  $\beta$ -diketiminato and acetylacetonate ligands [1]. A tautomeric structure for  $\beta$ -ketoiminate can be drawn for the ligand as shown below more accurately describing the bonding and charge distribution present in it. Even with several similarities, metal complexes of the  $\beta$ -ketoiminate ligand type have not been investigated in detail. With a preference to form four-coordinate metal compounds [1,2], a resistance to undergo polymerization [2–3], an easy route for changing steric interactions (by varying R and  $\text{R}\alpha,\beta,\gamma$ ) [1,2], and conformational flexibility which allows the metal complexes to undergo planar to tetrahedral conversions [4–6], the monoanionic  $\beta$ -ketoiminate ligand is unique and has experienced a resurgence in inorganic and organometallic chemistry as a scaffold for metal catalyzed reactions [7]. Particular attention has recently been focused on the roles of  $\beta$ -ketoiminate complexes as active site models for metalloenzymes [8], catalysts in polymerization [9], and other C–C bond forming reactions [10].



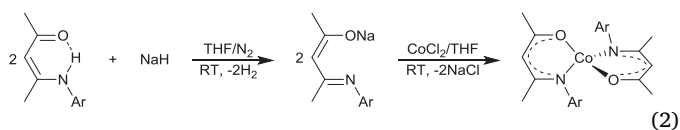
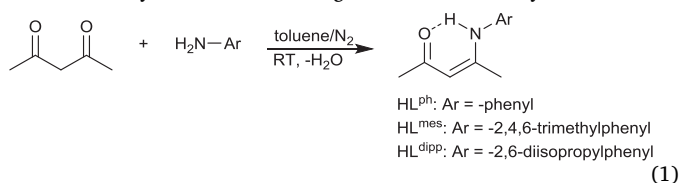
In comparison to the  $\beta$ -ketoiminate complexes of many other transition metals [1,2], cobalt(II)  $\beta$ -ketoiminate complexes have received relatively little attention, and the effect of electronic and steric effects present in ligand systems on their Co(II) complexes remains poorly understood. In one of the earlier studies, Holm and coworkers have investigated a series of cobalt(II) complexes of bidentate  $\beta$ -ketoiminate ligands  $\text{HL}^{\text{R}}$ ,  $\text{CH}_3\text{C}(\text{=O})\text{CH}=\text{C}(\text{NHR})\text{CH}_3$ , where  $\text{R} = \text{-H, -CH}_3, \text{-}^i\text{Pr, } n\text{-C}_3\text{H}_7$  and those of closely related tetradentate schiff base ligands [6]. This study has shown that the Co(II) complexes adopt pseudo-tetrahedral geometries and are high-spin. After Holm's study, research pertaining to Co(II)  $\beta$ -ketoiminates has remained dormant for over 40 years. Recently, Robson et al have studied a related series of aryl-substituted  $\beta$ -ketoamines,  $\text{PhC}(\text{=O})\text{CH}=\text{C}(\text{NHR})\text{CH}_3$ , where  $\text{R} = \text{aryl}$ ,

\* Corresponding author.

E-mail address: [sdebnath@uwyo.edu](mailto:sdebnath@uwyo.edu) (S. Debnath).

and note that the ligands also form tetrahedral Co(II) complexes [11]. Significantly, the redox properties of the new series of complexes are found to be sensitive to the presence of sterically-demanding aryl substituents.

As part our research efforts toward the synthesis of catalysts of earth abundant metals for small molecule activation, we have identified  $\beta$ -ketoiminates as a suitable ligand system for the modulation of the geometrical and electronic attributes of transition metal complexes. In this work, we employ three  $\beta$ -ketoiminates with varying extents of steric encumbrance and donor strengths. As shown in Eqs. 1 and 2, the ligands encompass both steric and electronic variation at the N-aryl group allowing us to study the influence of both of these factors in the reactivity of the Co(II) center. We have previously demonstrated that while the  $\beta$ -ketoiminate ligand systems are capable of enforcing strictly four-coordinate geometry around Fe(II) and Zn(II) ions, the highly sterically encumbered  $L^{\text{dipp}}$  ligand is also capable of forming a five-coordinate Fe(II) complex [12]. The unexpected coordination properties of  $L^{\text{dipp}}$  appears to result from the unique steric and electronic effects induced by the isopropyl substituents present in the N-aryl group. Hoping that the flexible protonation/deprotonation behavior of the ligand can further be exploited in small molecule activation, we have extended our investigation to include Co(II). For comparison, we have also studied the Co(II) complexes of the closely related  $L^{\text{ph}}$  and  $L^{\text{mes}}$  ligands. As will be discussed in the later sections, the Co(II) complex of  $L^{\text{dipp}}$  exhibits yet another form of geometrical flexibility.



## 2. Experimental

All manipulations were carried out using standard glove box techniques under a dinitrogen atmosphere. All reagents and solvents were obtained from commercial vendors and used as received. Tetrahydrofuran (THF), toluene, and diethyl ether were distilled under nitrogen gas from Na/benzophenone and subsequently stored over activated alumina. Acetonitrile and dichloromethane were distilled from calcium hydride under  $N_2$ . Non-halogenated solvents were typically tested with a standard purple solution of sodium benzophenone ketyl in tetrahydrofuran to confirm effective oxygen and moisture removal. Chemical reactions were all performed at high altitude (~7200 feet or ~2200 m).

Elemental Analyses were carried out at Columbia Analytical Services, Inc., Tucson, AZ. Electronic spectra (UV–Vis) were recorded on an Agilent 8453 diode-array spectrophotometer (250–1100 nm) which was equipped with a liquid nitrogen cryostat (Unisoku). Near IR UV–Vis absorption spectra were measured with a Cary 500 Scan UV–Vis-NIR spectrophotometer (250–3300 nm) (Varian Instruments). A quartz cell with 10 mm optical path length was used. The IR spectra were recorded as KBr pellets at room temperature on a Varian 800 FTIR (Scimitar Series) set to  $1\text{ cm}^{-1}$  resolution. Electrochemical measurements were carried out in a dry box under  $N_2$  in THF solution with 0.4 M ( ${}^t\text{Bu}_4\text{N}$ )( $\text{ClO}_4$ ) as the supporting electrolyte using a model ED-401 computer controlled potentiostat (eDAQ). A three-electrode configuration with a glassy carbon working electrode, a Ag wire reference electrode, and a platinum wire auxiliary electrode was used. The redox potential values were referenced to an internal ferrocenium/ferrocene

couple which is reported to be  $+0.53\text{ V}$  vs SCE in [ ${}^t\text{Bu}_4\text{N}$ ]( $\text{ClO}_4$ ) in THF [13]. The peak separations were reported with a scan rate of  $200\text{ mV/s}$  (the observed  $\text{Fc}^+/\text{Fc}^0$  peak separation was  $90\text{ mV}$  under these conditions).

Low resolution electrospray ionization mass spectral data (ESI-MS) for the complexes were obtained using an LCQ mass spectrometer (Finnigan MAT) for THF solutions that were directly infused into the spectrometer via a syringe pump. The heated capillary was set at  $150\text{ }^\circ\text{C}$ . Magnetic measurements were recorded for 45–55 mg crystalline samples using a Quantum Design Corp. SQUID variable-temperature susceptometer. The field dependence was measured and found to be linear from 5 to 25 kg. Sample measurements were made from 5 to 300 K at a magnetic field strength of 1000 Oe in a Lilly Gel Cap. Molar susceptibilities for the complex were calculated following corrections for bucket paramagnetism and underlying atomic diamagnetism.

Ligands,  $\text{HL}^{\text{ph}}$  (R = -phenyl),  $\text{HL}^{\text{mes}}$  (R = -mesityl) and  $\text{HL}^{\text{dipp}}$  (R = -diisopropylphenyl) were prepared following literature methods [7,12]. Attempted complexation reactions between the deprotonated ligands and  $\text{CoCl}_2$  in THF/acetonitrile solvents were unsuccessful. In one of the syntheses with  $\text{HL}^{\text{dipp}}$ , the sodium salt of the ligand was isolated instead of the desired Co(II) complex. Subsequently, the sodium salt was prepared as follows. NaH (0.048 g, 2.00 mmol) was added to a solution of  $\text{HL}^{\text{dipp}}$  (0.519 g, 2.01 mmol) in THF and stirred until the evolution of hydrogen ceased. The mixture was evaporated to dryness, and the solid obtained was dissolved in acetonitrile and layered with diethyl ether. Colorless crystals of  $[\text{Na}(\text{L}^{\text{dipp}})(\text{CH}_3\text{CN})]_4$  formed were filtered and dried. Yield: 0.124 g (0.278 mmol, 27.8%). Anal Calcd.  $\text{C}_{19}\text{H}_{27}\text{N}_2\text{NaO}$ : C, 70.78; H, 8.44; N, 8.69. Found: C, 70.76; H, 8.56; N, 8.40. ESI/MS (THF,  $150\text{ }^\circ\text{C}$ ):  $m/z = 282.1$  ( $[\text{M}]^+ = [\text{Na}(\text{HL}^{\text{dipp}})]^+$ ). When the reactions were carried out exclusively in THF, the respective Co(II) complexes were isolated.

$\text{Co}(\text{L}^{\text{ph}})_2$ . NaH (0.048 g, 2.00 mmol) was added to a solution of  $\text{HL}^{\text{ph}}$  (0.351 g, 2.00 mmol) in THF and stirred until the evolution of hydrogen ceased.  $\text{CoCl}_2$  (0.128 g, 0.992 mmol) was added and the mixture was stirred vigorously for 12 h. The reaction mixture was filtered to remove the inorganic salts. The filtrate was allowed to evaporate slowly when dark brown blocks formed. Yield: 0.285 g (0.70 mmol, 69.2%). Anal Calcd.  $\text{C}_{22}\text{H}_{24}\text{CoN}_2\text{O}_2$ : C, 64.86; H, 5.94; N, 6.88. Found: C, 64.58; H, 5.82; N, 6.54. UV–vis,  $\lambda_{\text{max}}$ , nm ( $\epsilon$ ,  $\text{M}^{-1}\text{cm}^{-1}$ ) in THF: 260 (9,500), 326 (42,000), 410 (924), 520 (62), 925 (55). ESI/MS (THF,  $150\text{ }^\circ\text{C}$ ):  $m/z = 407.13$  ( $[\text{M}]^+ = \text{Co}(\text{L}^{\text{ph}})_2^+$ ).

$\text{Co}(\text{L}^{\text{mes}})_2$ . NaH (0.049 g, 2.04 mmol) was added to a solution of  $\text{HL}^{\text{mes}}$  (0.435 g, 2.00 mmol) in THF and stirred until the evolution of hydrogen ceased.  $\text{CoCl}_2$  (0.128 g, 0.992 mmol) was added and the mixture was stirred overnight. The solvent was removed from the resultant dark brown solution, and the residue dissolved in toluene. Filtration yielded a brown solution which was evaporated to dryness. Upon layering a concentrated solution of the residue with acetonitrile brown crystals formed. Yield: 0.278 g (0.56 mmol, 47.4%). Anal Calcd.  $\text{C}_{28}\text{H}_{36}\text{CoN}_2\text{O}_2$ : C, 68.42; H, 7.38; N, 5.70. Found: C, 68.30; H, 7.30; N, 5.48. UV–vis,  $\lambda_{\text{max}}$ , nm ( $\epsilon$ ,  $\text{M}^{-1}\text{cm}^{-1}$ ) in THF: 300 (23,000), 510 (120), 405 (976), 945 (62), 1236 (58). ESI/MS (THF,  $150\text{ }^\circ\text{C}$ ):  $m/z = 491.13$  ( $[\text{M}]^+ = [\text{Co}(\text{L}^{\text{mes}})_2]^+$ ).

$\text{Co}(\text{L}^{\text{dipp}})_2$ . NaH (0.047 g, 1.99 mmol) was added to a solution of  $\text{HL}^{\text{dipp}}$  (0.517 g, 1.99 mmol) in THF and stirred until the evolution of hydrogen ceased.  $\text{CoCl}_2$  (0.128 g, 0.98 mmol) was added and the mixture was stirred overnight. The solvent was removed from the resultant dark brown solution and the residue dissolved in toluene. A brown solution was isolated via filtration of the inorganic salts. After evaporating toluene under  $N_2$  atmosphere, the solid was dissolved in THF and layered with acetonitrile. Orange brown crystals were obtained by slow evaporation of the THF/acetonitrile solution. Yield: 0.348 g (0.60 mmol, 60%); Anal Calcd.  $\text{C}_{34}\text{H}_{48}\text{CoN}_2\text{O}_2$ : C, 70.87; H, 8.40; N, 4.86. Found: C, 70.68; H, 8.43; N, 5.16. UV–vis,  $\lambda_{\text{max}}$ , nm ( $\epsilon$ ,  $\text{M}^{-1}\text{cm}^{-1}$ ) in THF: 310 (22,000), 500 (88), 542 (102), 973 (57), 1280 (50). ESI/MS (THF,  $150\text{ }^\circ\text{C}$ ):  $m/z = 575.1$  ( $[\text{M}]^+ = [\text{Co}(\text{L}^{\text{dipp}})_2]^+$ ). IR (KBr,

$\text{cm}^{-1}$ ): 3080  $\nu(\text{N-H})$ , 2959  $\nu(\text{C-H})$ , 1564 ( $\nu(\text{C}=\text{C})$ ), 1506  $\nu(\text{C}=\text{N})$ .

**X-ray diffraction analysis.**  $[\text{Na}(\text{L}^{\text{dipp}})(\text{CH}_3\text{CN})]_4$ ,  $\text{Co}(\text{L}^{\text{ph}})_2$ ,  $\text{Co}(\text{L}^{\text{mes}})_2$ , and  $\text{Co}(\text{L}^{\text{dipp}})_2$  and were characterized by single crystal X-ray diffraction data. Crystals of the compounds were glued to MiTeGen micro-mounts using Paratone N oil and mounted on a Bruker SMART APEX II CCD area detector system equipped with a graphite monochromator and a Mo K $\alpha$  fine-focus sealed tube operated at 1.5 kW power (50 kV, 30 mA). The data were measured for  $[\text{Na}(\text{L}^{\text{dipp}})(\text{CH}_3\text{CN})]_4$ ,  $\text{Co}(\text{L}^{\text{mes}})_2$  and  $\text{Co}(\text{L}^{\text{dipp}})_2$  at 150 K.  $\text{Co}(\text{L}^{\text{ph}})_2$  undergoes phase transition at low temperatures, and no satisfactory unit cell could be determined at 150 K. Fortunately, a data set measured at room temperature solves in a straightforward fashion. X-ray diffraction data were also measured at 100, 200 and 296 K for  $\text{Co}(\text{L}^{\text{dipp}})_2$ .

A series of narrow frames of data were collected with a scan width of  $0.5^\circ$  in  $\omega$  or  $\Phi$  and an exposure time of 10 s per frame. For each of the data sets, optimized data collection strategies were defined using the COSMO software program (APEX2 Software Suite v. 2.1–0, Bruker, AXS: Madison, WI, 2005). The data were corrected for absorption effects by the multi-scan method (SADABS). A summary of the crystallographic details is given in Table S1. The structures were solved by direct methods using the Bruker SHELXTL (v. 6.14) software program included in the Bruker Apex 2 software package. Patterson methods were used to solve the structures. In all of the structures, the non-hydrogen atoms were located in successive Fourier maps and refined anisotropically. The H atoms in  $[\text{Na}(\text{L}^{\text{dipp}})(\text{CH}_3\text{CN})]_4$  were placed in calculated positions and refined isotropically adapting a riding model. The hydrogen atoms of the acetonitrile solvate were neither located nor placed in calculated positions. In  $\text{Co}(\text{L}^{\text{ph}})_2$ , the two methine H atom of the chelate rings were located in the Fourier maps and refined isotropically. In  $\text{Co}(\text{L}^{\text{mes}})_2$ , the H atoms of the aromatic and chelate ring C–H were located in the Fourier maps and refined isotropically. The rest of the hydrogen atoms in both of the structures were placed in calculated positions and refined isotropically adapting a riding model. All of the H atoms in the four structure of  $\text{Co}(\text{L}^{\text{dipp}})_2$  determined at 100, 150, 200 and 296 K were placed in calculated positions, and refined isotropically as above.

$[\text{Na}(\text{L}^{\text{dipp}})(\text{CH}_3\text{CN})]_4$  crystallizes in the chiral tetragonal space group  $P4_21c$ . The asymmetric unit consists of a sodium cation, an  $\text{L}^{\text{dipp}}$  anion and a solvated acetonitrile molecule. The cation and anion are located on general positions and are well ordered, whereas acetonitrile molecule is disordered with located on a two-fold symmetry axis as the methyl carbon atom is located on the axis. The acetonitrile is also disordered occupying two positions. A free variable refinement settles at to ca. 50% occupancy for the two sites. Attempts to determine the absolute structure were unsuccessful as the crystal exhibits racemic twinning [14].

Crystals of  $\text{Co}(\text{L}^{\text{ph}})_2$  undergo crystalline phase transitions at low temperatures, and no satisfactory unit cell could be determined from data measured at 150 K. Therefore, a data set was measured at room temperature (296 K). The crystal belongs to the chiral orthorhombic space group  $Pna2_1$ . The absolute structure was satisfactorily refined by refining the Flack parameter to 0.010(16).

$\text{Co}(\text{L}^{\text{mes}})_2$  crystallizes in the centrosymmetric monoclinic space group  $P2_1/n$ . The asymmetric unit consists of a half of the molecule as the metal center is situated on an inversion center, and the molecule is well ordered.

Three of the data sets measured for  $\text{Co}(\text{L}^{\text{dipp}})_2$  at 150, 200 and 296 K belong to the same centrosymmetric monoclinic space group  $C2/c$  (Table S2). The structures are solved and refined similarly. The asymmetric unit in each of the structures consists of a half of the complex molecule with the metal center being situated on an inversion center. All atoms except for the ligating O atom are well ordered. The O atom was assigned two sites, and their occupancies refined by applying a free variable refinement. The free variable refines to 0.57 for the data sets measured at 150 K. The disordered O atom reflects the presence two isomers of  $\text{Co}(\text{L}^{\text{dipp}})_2$  in 57:43 ratio at 150 K. The overall refinement of

the structures from the 200 and 296 K data sets also progress well, however, the free variables refine to 0.66 and 0.76 indicating occurrence of the two isomers in 66:34 and 76:24 ratios at 200 and 296 K, respectively.

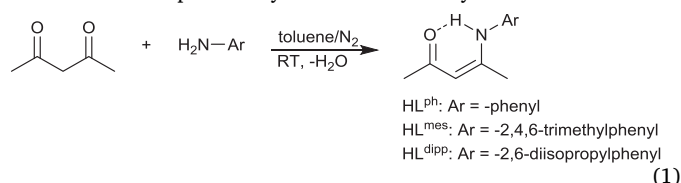
The 100 K data set does not solve well in  $C2/c$ , and despite our best efforts no satisfactory refinement could be achieved. However, the data set solves very well in the less-symmetric  $C2$  space group. The asymmetric unit consists of two well-ordered halves of  $\text{Co}(\text{L}^{\text{dipp}})_2$  molecules with the cobalt centers being located on inversion centers. The two four-coordinate  $\text{Co}(\text{II})$  complexes differ from each other due to the varying levels of distortion from tetrahedral geometry.

One crystal specimen was used for the measurement of the four data sets at 296, 200, 150 and 100 K. The transition between space groups is reversible, as another data set measured at 296 again solves in  $C2/c$  giving identical refinement parameters.

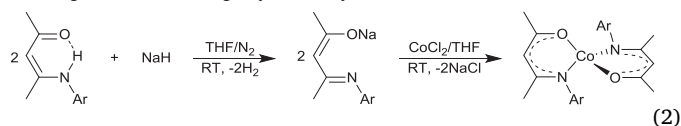
### 3. Results and discussion

#### 3.1. Syntheses

**Ligand and Complex Syntheses.** The ligands employed in this investigation were synthesized by condensing the appropriate  $\beta$ -diketone with a primary amine in presence of catalytic amount of *p*-toluenesulfonic acid under reflux (eq (1)). The resulting  $\alpha$ ,  $\beta$ -unsaturated- $\beta$ -ketoamines were purified by distillation or recrystallization in hexane.



An attempted synthesis of the  $\text{Co}(\text{II})$  complexes of the ligands by the reaction between freshly deprotonated ligands in THF using NaH and  $\text{CoCl}_2$  dissolved in acetonitrile were unsuccessful. The syntheses invariably led to the isolation of the sodium salt of the ligands. One of them, namely, the sodium salt of  $\text{HL}^{\text{dipp}}$ , was isolated as a crystalline solid. The product was characterized as  $[\text{Na}(\text{L}^{\text{dipp}})(\text{MeCN})]_4$  by crystallographic data. The structure reveals a network of 4 pairs of strongly interacting  $\text{Na}^+$  and  $[\text{L}^{\text{dipp}}]^-$  ions forming a distorted-cubic core. We assume that the formation of network is likely facilitated by acetonitrile and that the network formation precludes complexation of the ligand with  $\text{Co}(\text{II})$ . When the syntheses were carried out in THF solvent exclusively, the  $\text{Co}(\text{II})$  complexes are formed in moderate yield (Eq. 2). Crystals of  $\text{Co}(\text{L}^{\text{ph}})_2$  are obtained from the slow evaporation of the reaction mixture in THF during the synthesis of the complex in a glovebox, whereas those of  $\text{Co}(\text{L}^{\text{mes}})_2$  and  $\text{Co}(\text{L}^{\text{dipp}})_2$  were grown by the slow diffusion of acetonitrile into toluene solution of the complexes in the glove box. In the presence of air, the solutions change in color from brown or orange brown to blue or dark green within 2–3 h, and form a dark brown powder. As solids, the complexes are stable under ambient conditions for several days, but they begin to decompose after 1 week turning blue and losing crystallinity.



#### 3.2. Description of structures

$[\text{Na}(\text{L}^{\text{dipp}})(\text{MeCN})]_4$ . A view of the salt is shown in Fig. 1. The structure contains a cubane-like core featuring alternating sodium and oxygen atoms. Such cores are known in the structures of sodium salts of tetradentate Schiff base ligands [15]. The ligand anion in the present salt binds the sodium cation through its enolate O atom and imine N

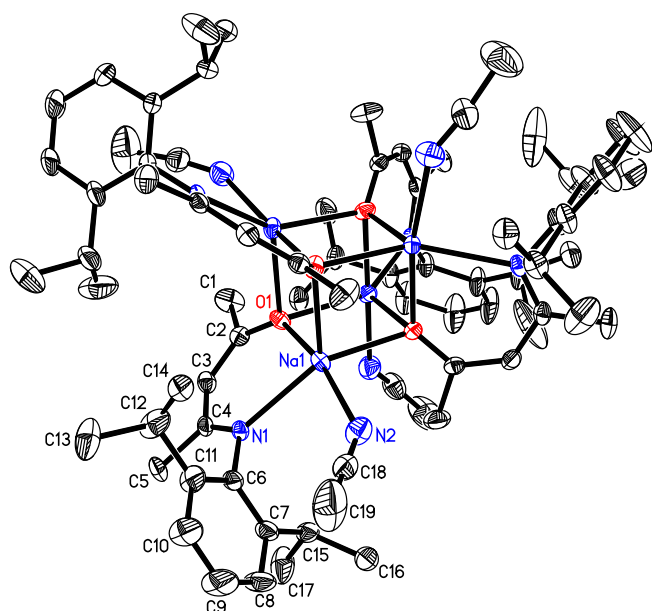


**Fig. 1.** View of the cubane-like structure in  $[\text{Na}(\text{L}^{\text{dipp}})(\text{CH}_3\text{CN})]_4$ . Only one of the two positions for the disordered acetonitrile molecules is shown. The thermal ellipsoids are drawn at 30% probability, H atoms are omitted and the symmetric equivalents are unlabeled in this and following Figure.

atom with the  $\text{Na}\cdots\text{O}$  and  $\text{Na}\cdots\text{N}$  bond distances of 2.255(2) and 2.466(7) Å, respectively. A set of 12 symmetrically equivalent  $\text{Na}\cdots\text{O}$  bonds for the 12 edges of the  $\text{Na}_4\text{O}_4$  pseudo-cubane were shown. The necessarily equivalent 8 faces of the core are planar with the diagonal  $\text{Na}\cdots\text{Na}$  and  $\text{O}\cdots\text{O}$  distances being 3.381(8) and 3.187(8) Å. Whereas the imine N atom is monodentate, the enolate oxygen atom acts as a tridentate ligand as it also binds two other sodium atoms with slightly longer  $\text{Na}\cdots\text{O}$  bond distances, 2.390(2) and 2.420(2) Å. Therefore, the sodium atom interacts with three  $\text{L}^{\text{dipp}}$  ligands forming a rectangular prismatic  $\text{Na}_4\text{O}_4$  unit-containing cluster. Each of the sodium centers also interact with a half of the disordered acetonitrile solvate with the associate  $\text{Na}\cdots\text{N}$  bond distance being 2.466(7) Å. The corresponding distance with the other half acetonitrile is considerably longer at 2.608(8) Å. The  $\text{OC}_3\text{N}$  chelate ring is nearly coplanar. The mean planes passing through the chelate ring and the phenyl ring of the ligand dissect each other at 86.98(11)°.

The strong macromolecular unit formed by 4 pairs of the sodium anion and  $\text{L}^{\text{dipp}}$  ligand anion leads to the association of the polar chelating ends of the ligand with the nonpolar framework forming a hydrophobic shell around the core. Interestingly, despite the presence of the sterically imposing isopropyl groups, the  $[\text{Na}(\text{L}^{\text{dipp}})(\text{MeCN})]_4$  macromolecules are tightly packed with no voids being present for even probe radius values as small as 0.9 Å. The absence of complexation with cobalt(II) salts, therefore, can be attributed to the tight packing.

$\text{Co}(\text{L}^{\text{ph}})_2$ ,  $\text{Co}(\text{L}^{\text{mes}})_2$  and  $\text{Co}(\text{L}^{\text{dipp}})_2$ . Crystals of  $\text{Co}(\text{L}^{\text{ph}})_2$  are found to undergo crystalline phase transition at low temperatures and  $\text{Co}(\text{L}^{\text{dipp}})_2$  to exhibit temperature dependent geometrical isomerization, whereas those of  $\text{Co}(\text{L}^{\text{mes}})_2$  are well behaved with so such behavior. Fortunately, a good quality diffraction data set could be measured for  $\text{Co}(\text{L}^{\text{ph}})_2$  at room temperature (296 K). A data set for  $\text{Co}(\text{L}^{\text{mes}})_2$  collected at 150 K was solved and refined in a straightforward manner. In contrast, a data set measured for  $\text{Co}(\text{L}^{\text{dipp}})_2$  at 296 K solves well, but the structure reveals the presence of two kinds of geometry for the Co(II) center. Therefore, three other data sets were also collected at 100, 150 and 200 K for  $\text{Co}(\text{L}^{\text{dipp}})_2$ . The molecular structures of  $\text{Co}(\text{L}^{\text{ph}})_2$  and  $\text{Co}(\text{L}^{\text{dipp}})_2$  at room temperature and that of  $\text{Co}(\text{L}^{\text{mes}})_2$  at 150 K are discussed here first, and the structures of  $\text{Co}(\text{L}^{\text{dipp}})_2$  at the various temperatures are compared later.

The coordination environment in the three complexes is similar

with each of the Co(II) centers being coordinated to two ligand anions through their enolate O and imine N atom pairs. Views of the complexes are given in Fig. 2, and selected structural parameters are listed in Table 1. Both  $\text{Co}(\text{L}^{\text{ph}})_2$  and  $\text{Co}(\text{L}^{\text{mes}})_2$  are well ordered. In  $\text{Co}(\text{L}^{\text{dipp}})_2$ , all atoms except for the ligating O atom are well ordered. The O is assigned two sites, and their occupancies refined applying a free variable. The free variable refines to 0.76 for the data set measured at 296 K. The disordered O atom reflects the presence of two isomers of  $\text{Co}(\text{L}^{\text{dipp}})_2$  in 76:24 ratio. A summary of crystallographic data for the low temperature structures are given in Table S2.

In  $\text{Co}(\text{L}^{\text{ph}})_2$  and  $\text{Co}(\text{L}^{\text{mes}})_2$  and in that of the larger component of  $\text{Co}(\text{L}^{\text{dipp}})_2$ , the metal centers are in pseudo tetrahedral geometry. The cobalt (II) centers are strictly tetra-coordinated as the closest Co–H–C distances in the complexes are > 3.15 Å ruling out any  $\text{Co}(\text{II})\cdots\text{H}$  agostic interactions. The bond angles at the cobalt center significantly deviate from 109° in all of the complexes revealing the distortion. The extent of distortion is quantified by calculating their  $\tau_4$  values (Table 1) as described by Houser et al [16], and the distortion is found to increase in the following order:  $\text{Co}(\text{L}^{\text{ph}})_2 < \text{Co}(\text{L}^{\text{mes}})_2 < \text{Co}(\text{L}^{\text{dipp}})_2$ . In all of the complexes, the  $\text{OC}_3\text{N}$  chelate rings formed by the ligands are nearly coplanar with the associated C–O, C–C and C–N bond distances associated being in the range of 1.279(3)–1.413(1) Å consistent with the delocalization of two double bonds throughout the chelate ring. The dihedral angles between the two chelate rings are close to 90° for  $\text{Co}(\text{L}^{\text{ph}})_2$  and  $\text{Co}(\text{L}^{\text{mes}})_2$ , but the angles in the two components of  $\text{Co}(\text{L}^{\text{dipp}})_2$  are significantly smaller. The large isopropyl substituents on the ligand's phenyl group clearly disfavor the near orthogonal configuration seen in the other two complexes. The dihedral angles between the chelate and phenyl ring planes also reflect the impact of the steric effect (Table 1); the angles are significantly small in  $\text{Co}(\text{L}^{\text{ph}})_2$  in comparison to those in  $\text{Co}(\text{L}^{\text{mes}})_2$  and  $\text{Co}(\text{L}^{\text{dipp}})_2$ . The observed near orthogonality of the aromatic  $\pi$ -systems relative to the respective chelate rings in these complexes negates any electron withdrawing resonance contribution from the phenyl rings. However, we expect that the +I effect due to the alkyl substituents will still operate, and the large isopropyl groups in the  $\text{L}^{\text{dipp}}$  anion clearly effects distortion from the ideal tetrahedral to square planar geometry in the solid state. The geometry of the second component of  $\text{Co}(\text{L}^{\text{dipp}})_2$  can be better described as a highly distorted square-planar. The corresponding dihedral angles in the closely related  $[\text{Fe}(\text{L}^{\text{dipp}})_2]$  and  $[\text{Zn}(\text{L}^{\text{dipp}})_2]$  are 59.41(3)° and 88.90(3)°, respectively [12]. Both these complexes show four-coordinate metal centers with bidentate  $\beta$ -ketoiminates and similar degrees of distortion on the basis of continuous symmetry measurements.  $[\text{Fe}(\text{L}^{\text{dipp}})_2]$  exhibits a seesaw or sawhorse geometry with a  $\tau_4$  value of 0.53.

The 150 and 200 K data sets measured for  $\text{Co}(\text{L}^{\text{dipp}})_2$  also solve in the same monoclinic space group,  $C2/c$ , and the overall refinement of the structures progress well. However, the free variable refinement of the disordered O atom refines to 0.57 and 0.66 indicating the occurrence of the two isomers in 57:43 and 66:34 ratios at 150 and 200 K, respectively. The 100 K data set solves in another monoclinic space group,  $C2$ , and contains two unique  $\text{Co}(\text{L}^{\text{dipp}})_2$  molecules. One of them is similar to the larger component structure determined from the 150, 200 and 296 K data sets, and the other is similar to the respective lower component structure. This can be interpreted to indicate that the ratio of the pseudo-tetrahedral and distorted square-planar molecules is 50:50. The  $\tau_4$  values calculated for the larger component molecules at 150, 200 and 296 K are 0.62, 0.61 and 0.62, respectively, and the  $\tau_4$  values for the smaller component are 0.27, 0.28 and 0.27, respectively. The  $\tau_4$  values for the two components in equal amounts at 200 are 0.64 and 0.26. These data reveal that essentially there are two geometrical isomers of  $\text{Co}(\text{L}^{\text{dipp}})_2$  existing at the various temperatures. The structures are interconvertible and the structure close to square planar geometry is preferred at lower temperatures. A sterically-driven square-planar, low-spin  $S = 1/2$  Co(II) configuration was recently observed in a bis(iminopyrrolyl)cobalt(II) species [17]. Square-planar cobalt(III) complexes bearing redox non-innocent aminophenolate or *o*-

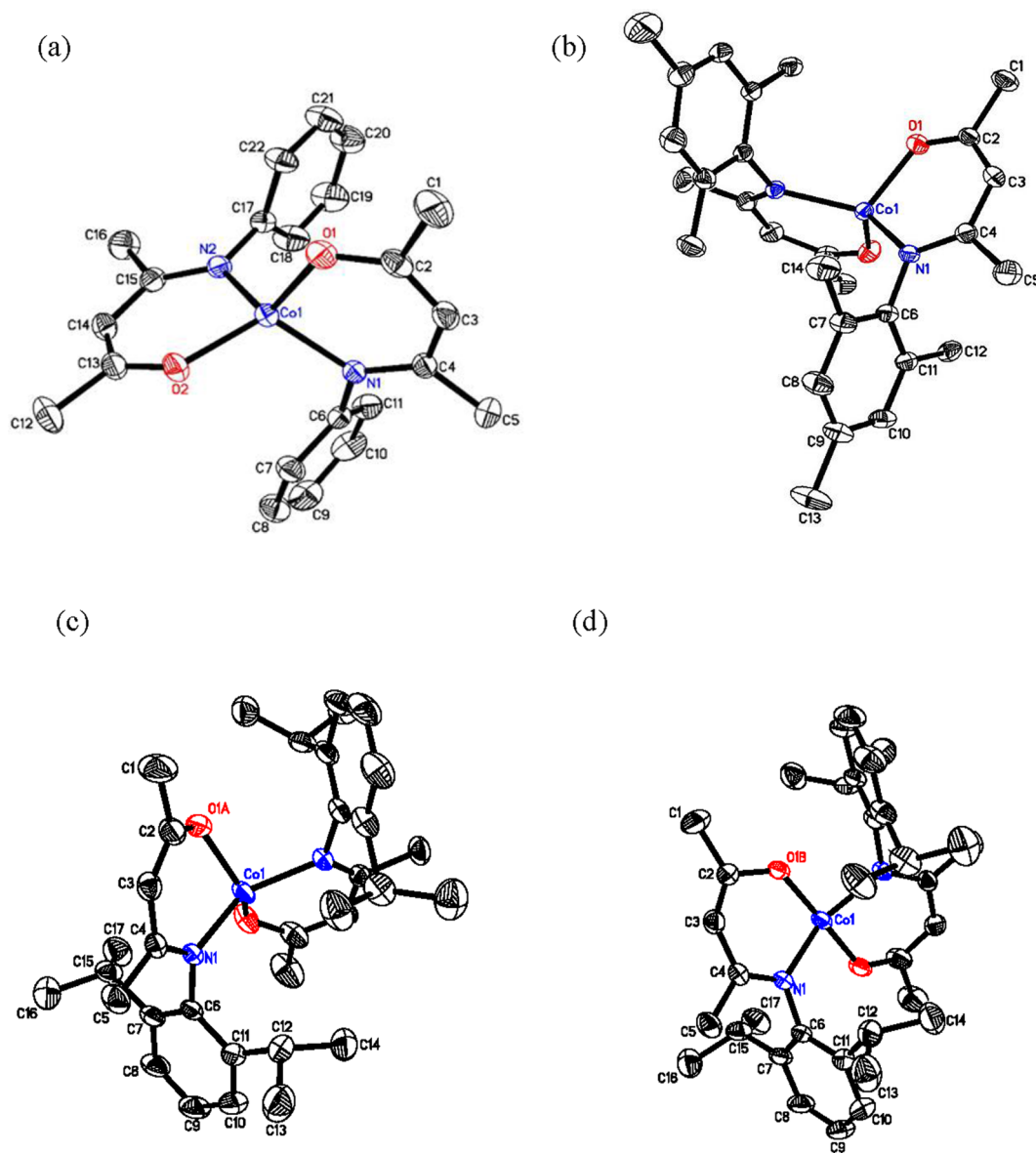


Fig. 2. Views of  $\text{Co}(\text{L}^{\text{ph}})_2$  (a),  $\text{Co}(\text{L}^{\text{mes}})_2$  (b), and the major (c) and minor isomers of  $\text{Co}(\text{L}^{\text{dipp}})_2$  at 296 K (d).

phenylenediamine groups are also known in the literature [18]. However, unlike the known complexes,  $[\text{Co}(\text{L}^{\text{dipp}})_2]$  exhibits fluxional geometries demonstrating the unique combination of steric and electronic effects in the  $\text{L}^{\text{dipp}}$  anion.

### 3.3. Description of physical properties

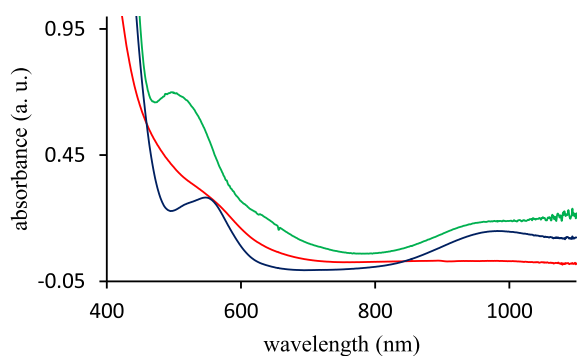
The cobalt(II)  $\beta$ -ketoiminate complexes show no noticeable color changes between the solid state and solution retaining their orange or brown color. The UV–vis spectra for  $\text{Co}(\text{L}^{\text{ph}})_2$ ,  $\text{Co}(\text{L}^{\text{mes}})_2$  and  $\text{Co}(\text{L}^{\text{dipp}})_2$  exhibit an intense absorption 300–326 nm consistent with literature precedent on other divalent  $\beta$ -ketoamine complexes [12]. Fig. 3 shows the spectra in the UV–vis region. The observed high extinction coefficients ( $\epsilon = 22,000\text{--}41,000 \text{ M}^{-1}\text{cm}^{-1}$ ) lead us to assign this band to two overlapping transitions of the ligand based  $\pi\text{--}\pi^*$  and metal-to-ligand charge transfer. In the visible region, a poorly resolved broad shoulder at ca. 410 nm ( $\epsilon = 924 \text{ M}^{-1}\text{cm}^{-1}$ ) is observed for  $\text{Co}(\text{L}^{\text{ph}})_2$ . In contrast, the spectra for  $\text{Co}(\text{L}^{\text{mes}})_2$  and  $\text{Co}(\text{L}^{\text{dipp}})_2$  contain reasonably well-defined peaks. Specifically,  $\text{Co}(\text{L}^{\text{mes}})_2$  shows a shoulder centered at ca. 475 ( $120 \text{ M}^{-1}\text{cm}^{-1}$ ) and two low peaks in the NIR region at 10,500 ( $952 \text{ nm}$ ,  $62 \text{ M}^{-1}\text{cm}^{-1}$ ) and  $8,070 \text{ cm}^{-1}$  ( $1,239 \text{ nm}$ ,  $58 \text{ M}^{-1}\text{cm}^{-1}$ ).

The UV–vis and NIR spectra for  $\text{Co}(\text{L}^{\text{dipp}})_2$  exhibit a shoulder centered at ca. 540 nm ( $\epsilon = 102 \text{ M}^{-1}\text{cm}^{-1}$ ) and two weak bands at 10,300 ( $971 \text{ nm}$ ,  $50 \text{ M}^{-1}\text{cm}^{-1}$ ) and  $7,800 \text{ cm}^{-1}$  ( $1,280 \text{ nm}$ ,  $57 \text{ M}^{-1}\text{cm}^{-1}$ ).

The cobalt(II) center in tetrahedral geometry possesses two excited states, namely,  ${}^4\text{T}_2(\text{F})$  and  ${}^4\text{T}_1(\text{F})$ , derived from the free ion with the  ${}^4\text{F}$  term, and another excited state derived from the  ${}^4\text{P}$  term,  ${}^4\text{T}_1(\text{P})$  in the UV–vis–NIR region. The three excited states are accessible for the electrons present in the  ${}^4\text{A}_2(\text{F})$  ground state, and the three possible spin-forbidden transitions can be arranged in the following order of decreasing energy:  ${}^4\text{A}_2(\text{F}) \rightarrow {}^4\text{T}_1(\text{P}) > {}^4\text{A}_2(\text{F}) \rightarrow {}^4\text{T}_1(\text{F}) > {}^4\text{A}_2(\text{F}) \rightarrow {}^4\text{T}_2(\text{F})$  [19]. Therefore, the high energy shoulder and peaks observed at ca. 410, 475 and 540 nm for  $\text{Co}(\text{L}^{\text{ph}})_2$ ,  $\text{Co}(\text{L}^{\text{mes}})_2$  and  $\text{Co}(\text{L}^{\text{dipp}})_2$ , respectively are assigned to the  ${}^4\text{A}_2(\text{F}) \rightarrow {}^4\text{T}_1(\text{P})$  transition. As can be seen from Fig. 3, the transition is too broad for  $\text{Co}(\text{L}^{\text{ph}})_2$ , whereas it is reasonably well resolved for  $\text{Co}(\text{L}^{\text{mes}})_2$  and  $\text{Co}(\text{L}^{\text{dipp}})_2$ . We attribute it to the higher degree of distortion at the Co(II) center for the latter complexes in comparison to the less distorted tetrahedral ( $T_d$ ) geometry in  $\text{Co}(\text{L}^{\text{ph}})_2$ . It is well known that tetrahedral Co(II) complexes exhibit solvent dependent shifts in their  $\lambda_{\text{max}}$  positions [20]. The nearly perfect tetrahedral  $\text{Co}(\text{L}^{\text{ph}})_2$  may be less accessible to solvent interaction with its metal center, whereas the metal centers in  $\text{Co}(\text{L}^{\text{mes}})_2$  and  $\text{Co}(\text{L}^{\text{dipp}})_2$  are likely accessible to THF molecules

**Table 1**Selected structural data for Co(L<sup>ph</sup>)<sub>2</sub> at 296 K, Co(L<sup>mes</sup>)<sub>2</sub> at 150 K and Co(L<sup>dipp</sup>)<sub>2</sub> at 296 K.

	Co(L <sup>ph</sup> ) <sub>2</sub>	Co(L <sup>mes</sup> ) <sub>2</sub>	Co(L <sup>dipp</sup> ) <sub>2</sub> <sup>a</sup>	Co(L <sup>dipp</sup> ) <sub>2</sub> <sup>b</sup>
Co1-O1 (Å)	1.926(2)	1.9250(7)	1.951(3)	1.812(7)
Co1-O2 (Å)	1.919(2)	1.9250(7)	1.951(3)	1.812(7)
Co1-N1 (Å)	1.961(2)	1.9733(8)	1.9708(10)	1.9708(10)
Co1-N2 (Å)	1.964(2)	1.9733(8)	1.9708(10)	1.9708(10)
O1-Co1-O2 (°)	117.60(7)	111.43(5) <sup>c</sup>	130.5(5) <sup>a</sup>	176(2) <sup>d</sup>
O1-Co1-N1 (°)	96.77(7)	96.54(3)	93.88(7)	92.1(3) <sup>d</sup>
O2-Co1-N1 (°)	115.63(9)	111.35(3) <sup>c</sup>	101.1(2) <sup>a</sup>	89.2(4) <sup>d</sup>
O1-Co1-N2 (°)	115.94(9)	111.35(3) <sup>c</sup>	101.1(2)	89.2(4)
O2-Co1-N2 (°)	96.83(7)	96.54(3)	93.88(7)	92.1(3)
N1-Co1-N2 (°)	115.42(7)	129.80(5) <sup>c</sup>	146.6(7)	143.6(7)
dihedral angle between chelate planes	89.18(5)	84.37(2)	63.9(1)	37.9(3)
dihedral angle between chelate and phenyl planes	66.67(10),	88.22(3)	80.42(6)	82.20(7)
tetrahedral distortion, τ <sub>4</sub>	70.30(11)	0.89	0.84	0.62
			0.27	

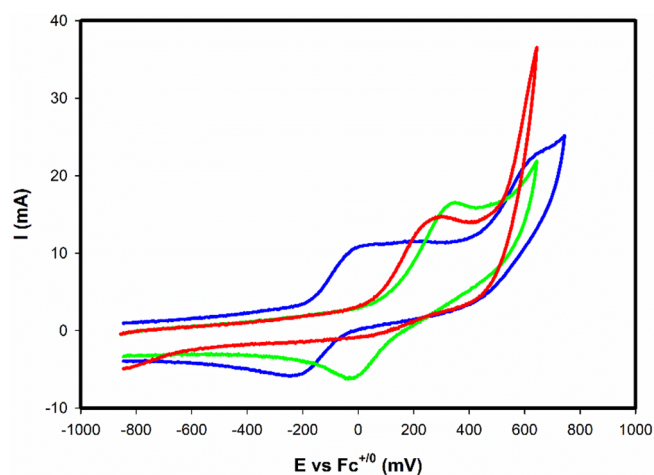
<sup>a</sup> O2 is the symmetric equivalent of O1.<sup>b</sup> For the larger component.<sup>c</sup> For the smaller component.<sup>d</sup> O1 = O1A and O2 is the symmetric equivalent of O1B.**Fig. 3.** UV-vis spectra in THF: Co(L<sup>ph</sup>)<sub>2</sub> (—), Co(L<sup>mes</sup>)<sub>2</sub> (—), and Co(L<sup>dipp</sup>)<sub>2</sub> (—).

in solutions. The NIR features observed for Co(L<sup>mes</sup>)<sub>2</sub> and Co(L<sup>dipp</sup>)<sub>2</sub> are comparable to those reported for high-spin cobalt(II) β-ketoiminate complexes at ca. 950 and 1,180 nm by Holm et al. [6], and to those reported for bis(N-arylsalicylaldimino)cobalt(II) complexes [21], which also contain Co(II) centers in pseudo-tetrahedral geometry. Therefore, the two NIR peaks are attributed to <sup>4</sup>A<sub>2</sub>(F) → <sup>4</sup>T<sub>1</sub>(F) and <sup>4</sup>A<sub>2</sub>(F) → <sup>4</sup>T<sub>2</sub>(F), with the low energy peak being assigned to the latter transition.

We also observe that all of the complexes are sensitive to the presence of air. The UV-vis spectra measured in the presence of air show a shift in the positions of the three peaks towards higher wavelengths. On standing for several hours, the solutions react with air to yield a green powder. Despite our best efforts the solids remain uncharacterized.

Cyclic voltammetric (CV) data were measured for THF and DCM solutions of the complexes in order to gain insight into likely solvent coordination. The peak potentials are given with respect to the ferrocene/ferrocinium, Fc<sup>0/+</sup> couple. The CV profiles measured for Co(L<sup>ph</sup>)<sub>2</sub> in THF contain an irreversible oxidation wave at +255 mV, while those of Co(L<sup>mes</sup>)<sub>2</sub> and Co(L<sup>dipp</sup>)<sub>2</sub> exhibit a quasi-reversible one-electron oxidation at +320 mV and -70 mV respectively (Fig. 4). We attribute the redox peaks to the Co(II) → Co(III) redox process. The shift of the Co<sup>2+/3+</sup> redox potentials to less positive values for Co(L<sup>dipp</sup>)<sub>2</sub> indicates that it is less likely to get oxidized. We interpret L<sup>dipp</sup> being a stronger field ligand than L<sup>ph</sup> and L<sup>mes</sup>, is capable of stabilizing the analogous Co(III) complex.

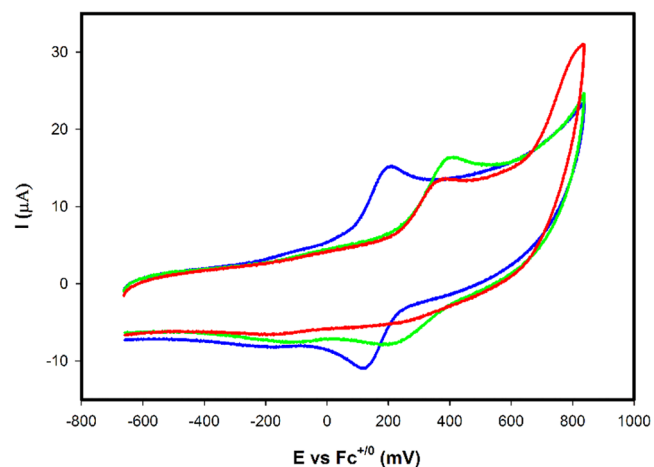
The electrochemical study was repeated using the generally non-coordinating DCM solvent. Although the general pattern of irreversible oxidation for Co(L<sup>ph</sup>)<sub>2</sub> and quasi-reversible oxidation of Co(L<sup>mes</sup>)<sub>2</sub> and

**Fig. 4.** Cyclic voltammograms for Co(L<sup>ph</sup>)<sub>2</sub> (—), Co(L<sup>mes</sup>)<sub>2</sub> (—), and Co(L<sup>dipp</sup>)<sub>2</sub> (—) in THF solutions (1.0 mM) containing [t<sup>+</sup>Bu<sub>4</sub>N](ClO<sub>4</sub>) (0.4 M) as the supporting electrolyte at a scan rate of 200 mV/s.

Co(L<sup>dipp</sup>)<sub>2</sub> is retained, the oxidation potentials are shifted significantly. The anodic peak for Co(L<sup>ph</sup>)<sub>2</sub> and the center of the quasi-reversible couple for Co(L<sup>mes</sup>)<sub>2</sub> are observed at +350 and +395 mV, respectively. A larger shift is observed for Co(L<sup>dipp</sup>)<sub>2</sub>, with its CV profile exhibiting a reversible couple at +190 mV (Fig. 5).

A comparison of the redox properties of the complexes in the two solvents reveals that the metal center in all of the complexes readily interact with THF, which is a better coordinating ligand than DCM. We propose that Co(II)⋯THF interaction plays a vital role in the overall electrochemical behavior of the complexes. The more open coordination environment in Co(L<sup>ph</sup>)<sub>2</sub> and Co(L<sup>mes</sup>)<sub>2</sub> allows for facile solvent coordination resulting in more positive oxidation potentials and less reversible electron transfer due to a readily available EC mechanism.

Qualitative magnetic susceptibility data were also measured for the cobalt(II) β-ketoiminate complexes to examine the spin state of the complexes. Effective magnetic moments of ca. 4.4 BM measured for Co(L<sup>ph</sup>)<sub>2</sub> and Co(L<sup>mes</sup>)<sub>2</sub> consistent with high-spin *d*<sup>7</sup> *S* = 3/2 configuration expected for Co(II) in a tetrahedral geometry [19]. Owing to the presence of a mixture geometrical isomers in the solid state, temperature dependent magnetic susceptibility measurements were carried out for Co(L<sup>dipp</sup>)<sub>2</sub> in the 5–300 K temperature range. As shown in Fig. 6, the effective magnetic moment (μ<sub>eff</sub>) is dependent on temperature and varies from 4.38 to 2.95 B. M., and the data also reveal that three

**Fig. 5.** Cyclic Voltammograms for Co(L<sup>ph</sup>)<sub>2</sub> (—), Co(L<sup>mes</sup>)<sub>2</sub> (—), and Co(L<sup>dipp</sup>)<sub>2</sub> (—) in DCM solutions (1.0 mM) containing [t<sup>+</sup>Bu<sub>4</sub>N](ClO<sub>4</sub>) (0.4 M) as the supporting electrolyte at a scan rate of 200 mV/s.

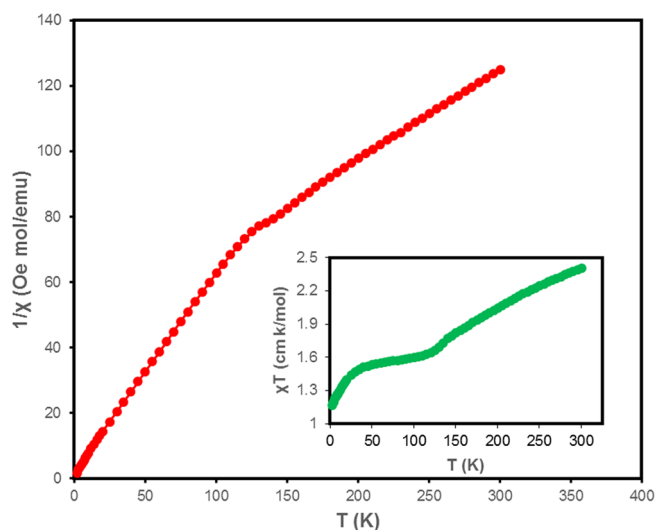


Fig. 6. Magnetic susceptibility plot of  $[\text{Co}(\text{L}^{\text{dipp}})_2]$ .

regions of unique rates for the change in molar susceptibility in the 300–125 K, 125–40 K and 40–5 K temperature ranges. Whereas in the first and second segments, there is a steady fall in  $(\chi_M)$  in the 150–125 K segment the value remains nearly flat in the 125–40 K region, and begins to fall in the third segment. The measured susceptibility values at 300 and 125 K correspond to  $\mu_{\text{eff}}$  values of 4.38 and 3.45 BM, and can be attributed to the presence of 3 and 1 unpaired electron(s), respectively. We interpret the magnetic susceptibility data to be reflective of the structural transition from high-spin tetrahedral to low-spin square-planar Co(II) geometries at low temperatures. In other words,  $\text{Co}(\text{L}^{\text{dipp}})_2$  undergoes  $S = 3/2$  (tetrahedral, high-spin)  $\leftrightarrow$   $S = 1/2$  (square-planar, low-spin) spin state transition in the 300–5 K temperature range with the complex preferring a square-planar geometry at  $T < 125$  K, tetrahedral geometry at  $T > 125$  K. The observed behavior is consistent with the crystallographic results obtained at 100 K. The ratio between the two conformations at 100 K (one more square planar, one more tetrahedral) in the solid state is 50/50, which indicate a magnetic moment in between the spin-only values for a pure  $S = 1/2$  and  $S = 3/2$  system.

#### 4. Conclusions

We have demonstrated the facile preparation of three cobalt(II)  $\beta$ -ketoiminate complexes with varying degrees of steric effects. Structural, spectroscopic and magnetic data reveal a unique interplay between the steric and electronic factors in cobalt(II) coordination chemistry. Increasing steric bulk and ligand field effect leads to unexpected distortion from tetrahedral geometry for  $\text{Co}(\text{L}^{\text{dipp}})_2$ . The complex undergoes gradual transition to the sterically favored tetrahedral geometry to the disfavored square planar geometry when cooled from room temperature to 100 K. Attendant changes in magnetic behavior are also measured for  $\text{Co}(\text{L}^{\text{dipp}})_2$  in the 300–5 K temperature range. The data are consistent with the transition and eventual conversion to the low-spin square-planar geometry at  $T < 40$  K. The redox characteristics of the complexes are also sensitive to steric factors. Distortion from tetrahedral geometry observed for  $\text{Co}(\text{L}^{\text{dipp}})_2$  allows the metal center significant solvent access. The shift of its  $\text{Co}^{2+/3+}$  redox peaks to more positive potentials in the less-coordinating dichloromethane solvent indicates that the metal ion interacts with solvent molecules or anions in solution. The fluxionality of the Co(II) geometry also indicates that the ligand system stabilizes a number of geometries around the metal ion. Solvent and substrate access to the Co(II) center and the metal ion's flexible geometry are valuable in catalysis, and further studies are

planned towards examining metal-substrate interactions involving suitable small molecules.

#### Acknowledgments

We thank the Department of Chemistry at the University of Wyoming and the Univ. of Wyoming School of Energy Research Graduate Assistantship to support this research. We also thank Prof. Parkinson for use of the Lambda 950 spectrophotometer. Financial supports by the NSF (CHE 0619920) for the purchase of the Bruker Apex II Diffractometer and National Institute of General Medical Sciences of the National Institutes of Health (from the Institutional Development Award, Grant no. 2P20GM103432) for the purchase of the Oxford Cryostream 800 cryogenic system are gratefully acknowledged.

#### Appendix A. Supplementary data

Supplementary data to this article can be found online at <https://doi.org/10.1016/j.ica.2018.10.051>.

#### References

- [1] R.H. Holm, G.W. Everett, A. Chakraborty, Metal complexes of Schiff bases and  $\beta$ -ketoamines, *Prog. Inorg. Chem.* 7 (1966) 83–214.
- [2] D.H. Gerlach, R.H. Holm, Solution stereochemistry of four-coordinate bis(chelate) metal(II) complexes. Further experimental results and a summary of stereochemical trends, *Inorg. Chem.* 9 (3) (1970) 588–594. [10.1021/ic50085a030](https://doi.org/10.1021/ic50085a030).
- [3] D.P. Graddon, G.M. Mockler, *Aust. J. Chem.* 17 (1964) 1119.
- [4] G.W. Everett, R.H. Holm, Comparative stereochemical populations and thermodynamics of structural interconversion of planar and tetrahedral cobalt(II) and nickel(II) complexes, *Inorg. Chem.* 7 (4) (1968) 776–785. <https://doi.org/10.1021/ic50062a032>.
- [5] G.W. Everett, R.H. Holm, Studies of the planar-tetrahedral configurational equilibrium in solutions of bis( $\beta$ -ketoamino)cobalt(II) complexes, *J. Am. Chem. Soc.* 88 (11) (1966) 2442–2451. <https://doi.org/10.1021/ja00963a016>.
- [6] G.W. Everett, R.H. Holm, The synthesis and proton resonance study of the solution equilibria of bis( $\beta$ -ketoamino) nickel(II) complexes, *J. Am. Chem. Soc.* 87 (10) (1965) 2117–2127. <https://doi.org/10.1021/ja01088a008>.
- [7] X. He, Y. Yao, X. Luo, J. Zhang, Y. Liu, L. Zhang, Q. Wu, Nickel(II) complexes bearing N, O-chelate ligands: synthesis, solid-structure characterization, and reactivity toward the polymerization of polar monomer, *Organometallics* 22 (24) (2003) 4952–4957. <https://doi.org/10.1021/om030292n>.
- [8] L. Bourget-Merle, M.F. Lappert, J.R. Severn, The chemistry of  $\beta$ -diketiminatometal complexes, *Chem. Rev.* 102 (9) (2002) 3031–3066. <https://doi.org/10.1021/cr010424r>.
- [9] A. Debuigne, J.-R. Caille, R. Jérôme, Highly efficient cobalt-mediated radical polymerization of vinyl acetate, *Angew. Chem. Int. Ed.* 44 (7) (2005) 1101–1104. <https://doi.org/10.1002/anie.200461333>.
- [10] W. Hess, J. Treutwein, G. Hilt, Cobalt-catalysed carbon-carbon bond-formation reactions, *Synthesis (Stuttg)* 2008 (22) (2008) 3537–3562. <https://doi.org/10.1055/s-0028-1083210>.
- [11] K.C.D. Robson, C.D. Phillips, B.O. Patrick, W.S. McNeil, Synthesis and characterization of bis( $\beta$ -ketoamino) complexes of cobalt(II), *Dalt. Trans.* 39 (10) (2010) 2573. <https://doi.org/10.1039/b921153e>.
- [12] D.M. Granum, P.J. Riedel, J.A. Crawford, T.K. Mahle, C.M. Wyss, A.K. Begej, N. Arulsamy, B.S. Pierce, M.P. Mehn, Synthesis and characterization of sterically encumbered  $\beta$ -ketoiminate complexes of iron(II) and zinc(II), *Dalt. Trans.* 40 (22) (2011) 5881. <https://doi.org/10.1039/c1dt10024f>.
- [13] N.G. Connelly, W.E. Geiger, Chemical redox agents for organometallic chemistry, *Chem. Rev.* 96 (2) (1996) 877–910. <https://doi.org/10.1021/cr940053x>.
- [14] R.S. Downing, F.L. Urbach, Circular dichroism of square-planar, tetradentate schiff base chelates of copper(II), *J. Am. Chem. Soc.* 91 (22) (1969) 5977–5983. <https://doi.org/10.1021/ja01050a009>.
- [15] E. Solari, S. De Angelis, C. Floriani, A. Chiesi-Villa, C. Rizzoli, Cubane structure of sodium derivatives of tetradentate schiff bases, *J. Chem. Soc. Dalt. Trans. No* (1991) 9 2471. [10.1039/dt9910002471](https://doi.org/10.1039/dt9910002471).
- [16] L. Yang, D.R. Powell, R.P. Houser, Structural Variation in Copper(I) complexes with pyridylmethylamide ligands: structural analysis with a new four-coordinate geometry index,  $\tau_4$ , *Dalt. Trans.* 9 (2007) 955–964. <https://doi.org/10.1039/B617136B>.
- [17] S.A. Carabineiro, L.C. Silva, P.T. Gomes, L.C.J. Pereira, L.F. Veiros, S.I. Pascu, M.T. Duarte, S. Namorado, R.T. Henriques, Synthesis and characterization of tetrahedral and square planar bis(iminopyrrolyl) complexes of cobalt(II), *Inorg. Chem.* 46 (17) (2007) 6880–6890. <https://doi.org/10.1021/ic062125w>.
- [18] E. Bill, E. Bothe, P. Chaudhuri, K. Chlopek, D. Herebian, S. Kokatam, K. Ray, T. Weyhermüller, F. Neese, K. Wieghardt, Molecular and electronic structure of four- and five-coordinate cobalt complexes containing two O-phenylenediamine- or two O-aminophenol-type ligands at various oxidation levels: an experimental,

- density functional, and correlated ab initio study, *Chem. A Eur. J.* 11 (1) (2005) 204–224, <https://doi.org/10.1002/chem.200400850>.
- [19] A.B.P. Lever, *Inorganic Electronic Spectroscopy*, Elsevier, 1984.
- [20] I. Kuźniarska-Biernacka, A. Bartecki, K. Kurzak, UV–Vis–NIR spectroscopy and colour of bis(N-phenylsalicylaldiminato)cobalt(II) in a variety of solvents, *Polyhedron* 22 (7) (2003) 997–1007, [https://doi.org/10.1016/S0277-5387\(03\)00028-7](https://doi.org/10.1016/S0277-5387(03)00028-7).
- [21] L. Sacconi, M. Ciampolini, F. Maggio, F.P. Cavasino, Studies in coordination chemistry. IX. 1 Investigation of the stereochemistry of some complex compounds of cobalt(II) with N-substituted salicylaldimines, *J. Am. Chem. Soc.* 84 (17) (1962) 3246–3248, <https://doi.org/10.1021/ja00876a005>.